Glycoconj J (2014) 31:231–245
DOI 10.1007/s10719-014-9517-y

Early stage fetal neocortex exhibits a complex ganglioside profile as revealed by high resolution tandem mass spectrometry

Roxana M. Ghiulai · Mirela Sarbu · Željka Vukelić · Constantin Ilie · Alina D. Zamfir

Received: 27 November 2013 / Revised: 5 February 2014 / Accepted: 10 February 2014 / Published online: 22 March 2014

Abstract In this study we report on the first mass spectrometric (MS) investigation of gangliosides and preliminary assessment of the expression and structure in normal fetal neocortex in early developmental stages: 14th (Neo14) and 16th (Neo16) gestational weeks. Ganglioside analysis was carried out using a hybrid quadrupole time-of-flight (QTOF) MS with direct sample infusion by nanoelectrospray ionization (nanoESI) in the negative ion mode. Under optimized conditions a large number of glycoforms *i.e.* 75 in Neo14 and 71 in Neo16 mixtures were identified. The ganglioside species were found characterized by a high diversity of the ceramide constitution, an elevated sialylation degree (up to pentasialylated gangliosides-GP1) and sugar cores modified by fucosylation (Fuc) and acetylation (*O*-Ac). Direct comparison between Neo14 and Neo16 revealed a prominent expression of monosialylated structures in the Neo16 as well as the presence of a larger number of polysialylated species in Neo14 which constitutes a clear marker of rapid development-dependant changes in the sialylation. Also the MS screening results highlighted that presumably *O*-acetylation process occurs faster than fucosylation. CID MS/MS under variable collision energy applied for the first time for structural analysis of a fucosylated pentasialylated species induced an efficient fragmentation with generation of ions supporting Fuc-GP1d isomer in early stage fetal brain neocortex.

Keywords Gangliosides · Neocortex · Nanoelectrospray · QTOF MS · CID MS/MS

Abbreviations

Ac	Acetyl/acetylation
Cer	Ceramide
gw	Gestational weeks
CID	Collision-induced dissociation
Neu5Ac	*N*-acetyl neuraminic acid
NanoESI	Nanoelectrospray ionization
MS	Mass spectrometry
MS/MS	Tandem mass spectrometry
TIC	Total ion chromatogram
QTOF MS	Quadrupole time-of-flight mass spectrometer/spectrometry
LM	Low mass resolution
HM	High mass resolution

Abbreviations used for gangliosides

LacCer	Galβ4Glcβ1Cer
GM3	II^3-α-Neu5Ac-LacCer
GD3	II^3-α-$(Neu5Ac)_2$-LacCer
GT3	II^3-α-$(Neu5Ac)_3$-LacCer
GM2	II^3-α-Neu5Ac-Gg_3Cer
GD2	II^3-α-$(Neu5Ac)_2$-Gg_3Cer
GM1a or GM1	II^3-α-Neu5Ac-Gg_4Cer

Roxana M. Ghiulai and Mirela Sarbu have equal contribution.

R. M. Ghiulai · C. Ilie
Department of Neonatology, University of Medicine and Pharmacy "Victor Babes", Eftimie Murgu Square 2, 300041 Timisoara, Romania

M. Sarbu · A. D. Zamfir (✉)
Department of Chemistry and Biology, "Aurel Vlaicu" University, Revolutiei Blvd. 77, 310130 Arad, Romania
e-mail: alina.zamfir@uav.ro

M. Sarbu
Department of Physics, West University Timisoara, Vasile Parvan Blvd. 4, 300223 Timisoara, Romania

Ž. Vukelić
Department of Chemistry and Biochemistry, University of Zagreb Medical School, 10000 Zagreb, Croatia

A. D. Zamfir
Mass Spectrometry Laboratory, National Institute for Research and Development in Electrochemistry and Condensed Matter, Plautius Andronescu 1, 300224 Timisoara, Romania

GM1b	IV^3-α-Neu5Ac-Gg_4Cer
GalNAc-GM1b	IV^3-α-Neu5Ac-Gg_5Cer
GD1a	IV^3-α-Neu5Ac,II^3-α-Neu5Ac-Gg_4Cer
GD1b	II^3-α-$(Neu5Ac)_2$-Gg_4Cer
GT1b	IV^3-α-Neu5Ac,II^3-α-$(Neu5Ac)_2$-Gg_4Cer
GQ1b	IV^3-α-$(Neu5Ac)_2$,II^3-α-$(Neu5Ac)_2$-Gg_4Cer
nLM1 or 3′-nLM1	IV^3-α-Neu5Ac-nLc_4Cer
LM1 or 3′-isoLM1	IV^3-α-Neu5Ac-Lc_4Cer
nLD1	disialo-nLc_4Cer

Introduction

The neocortex is the top layer of the cerebral hemispheres with a six layer structure, labeled from I to VI from the outermost to the innermost, and along with the archicortex and paleocortex, which are cortical parts of the limbic system, is part of the cerebral cortex [1, 2].

Neocortex consists of grey matter that surrounds the deeper white matter of the cerebrum. Neocortex architecture exhibits deep grooves (sulci) and wrinkles (gyri), characteristic folds that serve to increase the area of the neocortex considerably, resolving the problem of a large surface area in a small volume [3].

The neocortex is involved in higher functions such as sensory perception, generation of motor commands, spatial reasoning, conscious thought, speech production and comprehension [4]. The cortical neuron production begins by the 6th gestational week (gw); between the 11th and 17th gestational weeks the neuron production in the neurocortex is at full speed [1].

Gangliosides are a class of glycosphingolipids located in the outer layer of the plasma membrane. They are formed by a sialylated (mono/poly) oligosaccharide chain of variable length attached to a ceramide portion of different compositions in terms of the sphingoid base and fatty acid residues [5].

Gangliosides contain a hydrophobic moiety, represented by the ceramide, oriented to the inside of the membrane and a hydrophilic oligosaccharide moiety, which faces the external medium and enables them to interact with other soluble extra cellular molecules [6, 7]. Central nervous system (CNS) contains the highest amount of gangliosides, neuronal membranes holding ten times higher concentrations of gangliosides than the extraneural cell types, highlighting the special role of these molecules at the CNS level [8–11]. The ganglioside composition was demonstrated to change specifically during brain development, maturation, aging [12], and neurodegeneration [13, 14].

Gangliosides extracted from various fetal brain regions at different gestational stages in health or disease were investigated before by advanced mass spectrometry (MS) using platforms based on NanoMate robot in combination with either quadrupole time-of-flight (QTOF) or high capacity ion trap (HCT) mass spectrometers. Hence, the 15th and 40th gw fetal cerebellum [15], the white matter of the occipital lobe and frontal lobe [16], the 15th and 17th gw fetal hippocampus [17], the 28th gw anencephalic residual brain tissue (glial islands) and the 27th gw normal fetal frontal lobe [18] were thoroughly characterized with respect to their ganglioside profile. Also the native ganglioside mixtures extracted from the 36th gw frontal neocortex [16], were rather recently analyzed by fully automated chip-based nanoESI (Nanomate) ion trap MS and multistage MS. The comparisons between frontal, occipital lobes and neocortex have postulated that the dissimilarity in ganglioside expression in fetal brain depends mostly on the phylogenetic development and much less on the topographic factors. This feature, discovered exclusively by MS, highlights the major role of gangliosides in human brain evolution and advancement of its functions in comparison with other mammals. Moreover, these studies revealed that certain species are biomarkers of the fetal neocortex, being correlated to the particular functions of this brain region.

We report here on the first high resolution mass spectrometric analysis of native ganglioside mixtures extracted from normal fetal neocortex in an incipient developmental phase: in the 14th (Neo14) and 16th (Neo16) gestational week (gw).

The aim of this study is to provide a closer insight into the ganglioside expression in early stages of brain development *i.e*. neocortex as the newest region in mammals, and complete the information on the previously postulated association of gangliosides with the phylogenetic development.

The study was carried out using a hybrid QTOF MS with direct sample infusion by nanoelectrospray ionization (nanoESI) in the negative ion mode. The two ganglioside mixtures were characterized by nanoESI MS screening and tandem MS (MS/MS) using collision induced dissociation (CID) sequencing for Neo14 and Neo16 structural characterization of associated species.

Under optimized conditions we were able to detect a large number of glycoforms characterized by a high diversity of the ceramide constitution, structures with an elevated sialylation degree (up to pentasialylated gangliosides-GP1) and with sugar core modifications such as fucosylation (Fuc) and acetylation (*O*-Ac). By employing CID MS/MS we were able to fragment and structurally characterize for the first time the pentasialylated ganglioside Fuc-GP1(d18:1/18:0) a marker of the early neocortex development.

Materials and methods

Sampling of human cortex

The native ganglioside mixtures analyzed in this study were purified from fetal neocortex, in the 14th gestational week

(Neo14) and 16th gestational week (Neo16). Fetal brain samples were obtained during routine pedopathological section/autopsy examination at Clinical Hospital for Obstetrics and Gynecology "Petrova", Zagreb, Croatia. Both fetuses deceased because of spontaneous abortion. The age of the fetuses was established from the mother's menstrual history and the echographic fetal biometry conducted during pregnancy follow-up corroborated with specific measurements of the aborted fetuses such as the biparietal perimeter, the femoral length and the humerus length together with weight measurements.

No signs of brain malformation, aberrant development or injuries were found during pedopathological examination, including histopathological tissue analysis. Hence, the brains were considered normal for the respective gestational period. The brain samples were weighed and stored at −20 °C until the ganglioside extraction procedure. Permission for experiments with human tissues for scientific purposes was received from the Ethical Commission of the Zagreb Medical Faculty, under the Project no. 108120, financed by the Croatian Ministry of Science and Technology.

Ganglioside extraction and purification

Gangliosides were extracted and purified from Neo14 and Neo16 tissues. An identical mass of tissue of 0.6 g was used as the starting material for ganglioside extraction in both cases. The extraction and purification were performed under identical conditions for both samples and followed the procedures described before [19, 20] and the method developed by Svennerholm and Fredman [21] as modified by Vukelić *et al.* [22]. Prior to ganglioside extraction, the tissue was homogenized in ice-cold water. Lipids were extracted twice using chloroform-methanol–water mixture (1:2:0.75, by vol.). After centrifugation, to separate gangliosides from other lipids, the combined supernatant was submitted to a phase partition followed by repartition, by adding chloroform, methanol and water to a final volume ratio 1:1:0.8. Combined upper phases, containing polar glycosphingolipids (gangliosides) were collected. The crude ganglioside extract was purified in several steps: precipitation of co-extracted protein-salt complexes followed by centrifugation; low-molecular weight contaminants were removed by gel-filtration on Sephadex G-25 column and dialysis against water in an overnight procedure at 4 °C. To preserve possible physiologically-relevant alkali-labile species, no alkali-hydrolysis step was performed during purification. Finally, the pure extracts were evaporated to complete desiccation in a SpeedVac concentrator (SPD 111 V–230, Thermo Electron, Asheville, NC, USA) coupled to a vacuum pump (PC 2002 Vario with CVC 2000 controller, Vaccubrand, Wertheim, Germany). The obtained dry samples were weighed and stored at −27 °C.

HPTLC and laser densitometric quantification

The ganglioside mixtures isolated and purified from Neo14 and Neo16 were analyzed by high performance thin layer chromatography (HPTLC) and laser densitometry. Quantitative analysis of total ganglioside concentration was performed according to the spectrophotometric method of Svennerholm [23], as modified by Miettinen and Takki-Luukkainen [24]. The absorbance of the sample and Neu5Ac used as a standard in a range of known concentrations were determined at 580 nm; the concentration of ganglioside-bound sialic acids was expressed as microgram ganglioside-sialic acid per gram of fresh tissue wet weight (w.w) Qualitative analysis was performed by HPTLC separation of individual ganglioside fractions on glass backed HPTLC-plates (silica gel 60, 0.2 mm, 10×10 cm, Merck, Germany). The plates were developed in a solvent system containing chloroform, methanol and 12 mM $MgCl_2$ (58:40:9, v/v/v). After drying, the plate was sprayed with resorcinol reagent and heated for 30–45 min until GG fractions appeared as bluish bands. Finally, HPTLC separated and visualized ganglioside fractions were subjected to laser densitometric scanning (LKB 2202 Laser Ultrascan, LKB, Bromma, Sweden) at 580 nm, enabling relative quantification of individual gangliosides, expressed as their relative proportion (%) in the sample.

Sample preparation for MS

For QTOF MS analysis, a stock solution at 0.5 mg/mL concentration of each native ganglioside extract was prepared by dissolving the dried material in pure methanol. Methanol was obtained from Merck (Darmstadt, Germany) and used without further purification. Prior to MS analysis the stock solution was stored at −22 °C. Distilled and deionized water obtained by using a system from SG Water (Germany) was used for preparation of all sample solutions. Working aliquots at concentration of approximately 2 pmol/μL (calculated for an average molecular weight of 2,000) were obtained by dilution of the stock solution in a mixture of methanol/water (1:1 by vol.).

Prior to MS analysis, the sample solution was centrifuged for 1 h in a mini-centrifuge (6,000 rpm) from ROTH (Germany). The supernatant was collected and submitted to (−) nanoESI QTOF MS and MS/MS analysis by collision induced dissociation (CID) at low energies.

QTOF MS and CID MS/MS

Nano ESI experiments were carried out using self-pulled omega glass capillaries (Analytik Vertrieb, Germany) produced on a vertical pipette puller, model 720 (David Kopf Instruments, Tujunga, CA, USA) by an "omega" shape filament. The sample solution was loaded into the pulled glass capillary using gel loader tips from Eppendorf (Hamburg, Germany). A stainless steel wire connected to power supply

the Z-spray ion source was inserted into the capillary. ESI process was initiated by applying 1.8 kV voltage to the solution via the stainless steel wire.

MS and CID MS/MS were performed on a hybrid QTOF micro (Micromass/Waters, Manchester, UK) instrument with direct nanoESI infusion in the Micromass Z-spray geometry. QTOF MS is connected to a PC computer running the MassLynx 4.1 software to control the instrument, acquire and process MS data. For all acquisitions, the instrument was tuned to record the data at a scan speed of 1 scan/s. For each screening and fragmentation mass spectrum the signal was acquired for about 5 min. All mass spectra were recorded in the negative ion mode, which was previously demonstrated to be the best option for this type of molecules since gangliosides readily undergo deprotonation [25, 26]. For an efficient ionization and minimal in-source fragmentation, the cone voltage was varied within the range of 30–50 V. The desolvation gas was adjusted within 30–50 L/h range while the source block temperature was set to 80 °C and kept at this value during all experiments. MS/MS was performed by CID at low ion acceleration energies using argon at 12 psi pressure as the collision gas. For MS/MS, the ions were isolated by setting the LM and HM parameters to 10 and 10 respectively which provided a fair compromise between the precursor ion isolation and measurement sensitivity. The product ion spectrum represents a sum of scans combined over total ion current (TIC) acquired at variable collision energy within 30–60 eV range adjusted to provide the full set of fragment ions diagnostic for the respective structure.

The screening and fragmentation mass spectra were calibrated using as the reference a standard native mixture of bovine brain gangliosides "Cronassial", commercially available from Fidia Research Laboratories (Abano Terme, Italy). The reference provided in the negative ion mode a spectrum with a high ionic coverage of the *m/z* range scanned in both MS and CID MS/MS experiments. Gangliosides and the precursor glycosphingolipids are abbreviated according to the system introduced by Svennerholm [27] and the recommendations of IUPAC-IUB Commission on Biochemical Nomenclature (IUPAC-IUB 1998) [28]. The carbohydrate sequence ions were assigned according to the nomenclature introduced by Domon and Costello [29], while the fragment ions derived from the ceramide were denoted according to Ann and Adams [30].

Results and discussions

Quantification of Neo14 and Neo16 gangliosides by HPTLC and laser densitometry

The total ganglioside content in Neo14 and Neo16 sample was 298.85 and 310.16 μg, respectively of ganglioside-bound sialic acid per gram tissue w.w. (μg ganglioside-sialic acid/g), as determined by the spectrophotometric method. Qualitative analysis of ganglioside pattern in Neo14 and Neo16 tissues was performed using HPTLC (Fig. 1). According to the inspection of the HPTLC plates, ganglioside fractions migrating as GM3, GM2, GM1, GD3, GD1a, GD1b, GD2, GT1 and GQ1 were detected in both samples. The proportions of individual fractions separated by HPTLC were quantified by densitometric analysis as presented in Table 1.

Inspection of Table 1 shows that a number of differences between the proportions of ganglioside fractions in Neo14 and Neo16 exist. While GM3, GM2, GD3 and GD1b ganglioside fractions are similarly expressed quantitatively in the two samples, significant discrepancy in the proportions of GM1, GD1a, GD2, GT1 and GQ were found. Hence, the monosialylated species, GM1 accounts for 5.03 % of the total ganglioside content in Neo14 and for 29.73 % in Neo16. GT1 percentage in Neo14 is almost two times higher than in Neo16, while GQ1 precentage in Neo14 is about ten times higher. These data indicate that polysialylated species exhibit a higher abundance in Neo14.

Screening of Neo14 and Neo16 ganglioside mixtures

Ten μL sample solution of Neo14 and Neo16 ganglioside mixtures, extracted and purified from fetal neocortex tissue were loaded into the nanoelectrospray capillary and submitted to

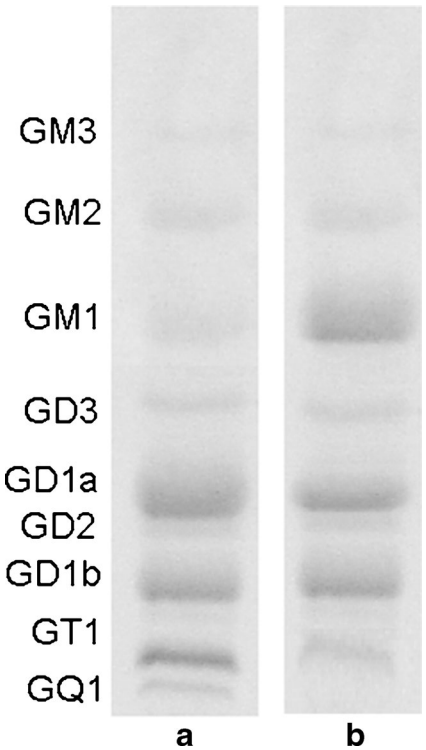

Fig. 1 HPTLC analysis of individual gangliosides from **a** Neo14 and **b** Neo16 samples. Solvent system: chlorophorm, methanol and 12 mM $MgCl_2$ (58:40:9, v/v/v). Detection limit 1 μg

Table 1 Proportion of HPTLC-separated ganglioside fractions quantified by densitometric analysis in Neo14 and Neo16 samples. Detection limit 1 μg

Ganglioside fraction	Proportion of individual gangliosides (%) in Neo 14	Proportion of individual gangliosides (%) in Neo 16
GM3	2.16	2.73
GM2	5.98	6.89
GM1	5.03	29.73
GD3	6.17	6.75
GD1a	27.69	14.92
GD2	9.73	3.26
GD1b	18.21	17.94
GT1	13.55	7.08
GQ1	5.21	0.61

negative nanoESI QTOF MS screening under identical solution and instrumental conditions. The parameters were adjusted and optimized to minimize the *in-source* fragmentation and produce a spectrum with high signal to noise ratio [31].

The spectra generated under the employed conditions for Neo14 and Neo16 sample solutions are depicted in Figs. 2 and 3, respectively. In view of the high number of signals, in order to enhance the differentiation of the detected ions, the structures corresponding to the *m/z* values from the two spectra are listed in Table 2.

A detailed evaluation of the two ESI QTOF mass spectra indicates that both Neo14 and Neo16 ganglioside mixtures present a rich molecular ion pattern. The optimized nanoESI QTOF MS conditions produced mono- doubly- and triply-charged ions, promoted the ionization of long-chain polysialylated GT, GQ and GP components and prevented the *in-source* fragmentation of labile sugar and non-sugar types of carbohydrate core decorations such as Fuc and *O*-Ac.

The two screening mass spectra reveal the presence of a large number of glycoforms and a high diversity of the ceramide constitution for certain compounds.

A total of 93 distinct gangliosides were detected in the two ganglioside mixtures, out of which 75 were found in the Neo14 sample and 71 in the Neo16 sample. Although the two native mixtures present a comparable number of gangliosides, important differences were observed in the sialylation degree, the occurrence of fucosylation, acetylation and the nature of the sphingoid base. Thus a number of 11 monosialogangliosides (GM) were detected in the Neo14 sample while in the Neo16 sample, 15 were detected. Disialo species (GD) were found also differently expressed. A number of 22 occur in the Neo14 sample and only 18 in the Neo16 sample. 32 and 27 trisialogangliosides (GT), were discovered in the Neo14 and Neo16 ganglioside mixtures respectively. An equal number of tetrasialogangliosides (GQ) namely 8, were detected in both samples. Pentasialogangliosides were almost the same expressed: 2 in the Neo14 and 3 in the Neo16 sample respectively.

Several fucosylated species, although not detectable in the HPTLC being bellow the detection limit, were detected by the high sensitivity and resolution of nanoESI QTOF MS. Hence 26 were found in the Neo14 and 23 in the Neo16 ganglioside mixture. As for the *O*-acetylated species, 6 in Neo14 and 7 in Neo16 sample were detected. The comparison between the two ganglioside mixtures is also interesting in what the nature of the sphingoid base concerns. Thus, 51 gangliosides having dihydroxylated sphingoid base were found in the Neo14 sample, while 47 in the Neo16 sample. 24 gangliosides having trihydroxylated sphingoid bases were discovered in both samples. The incidence in humans of ganglioside species exhibiting trihydroxylated sphingoid bases (t18:0) and (t18:1) was reported previously in epithelial cells of the small intestine [32] fetal hippocampus in the 17th g.w. [17], fetal frontal lobe in the 27th [18] and 36th [16] g.w. as well as in adult human cerebellum [19], and adult sensory and motor cortex [33]. Obviously, trihydroxylation of the sphigoid base is a process accompanying the human brain along the intrauterine and extrauterine development. A thorough analysis of the two spectra reveals the presence of 22 distinct gangliosides that were detected only in the Neo14 ganglioside mixture and were absent in the Neo16 sample. From the monosialo group, 4 species out of which 1 *O*-acetylated and 1 fucosylated were discovered: *O*-Ac-GM3(d18:0/20:0), GM2 (d18:1/16:2), GM1 (d18:1/24:2), Fuc-GM1 (d18:1/18:0). A number of 5 disialylated glycoforms were present only in the Neo14 sample of which 1 fucosylated: GD2 (d18:1/24:0), GD1 (t18:1/20:1), GD1 (d18:1/22:0), GD3 (d18:1/18:0) and Fuc-GD1 (t18:1/20:0). 11 trisialogangliosides including 5 fucosylated were detected only in the Neo14 sample: GT1(t18:1/18:2), GT1(d18:1/16:1), Fuc-GT2(d18:1/20:0), GT1 (d18:1/20:0), GT1(t18:1/18:2), Fuc-GT1(t18:1/24:0), GT3(t18:1/20:0), GT3(d18:1/24:0), Fuc-GT3 (t18:1/24:4), Fuc-GT2 (t18:1/16:4) and Fuc-GT2 (t18:1/18:2).

Neo16 ganglioside mixture also contains a number of 18 species, identified through their molecular ions of fair abundance, that are completely absent in the Neo14 sample. The monosialogangliosides group is the dominant one, encompassing different glycoforms such as: GM4 (t18:0/18:0), GM4 (d18:1/20:2), GM4(d18:1/22:2), *O*Ac-GM4(d18:1/22:03), GM3(t18:1/18:2), GM3(d18:1/22:0), GM3(d18:1/24:0), GM1 (d18:0/24:0). Interestingly, the low aboundant GM4 group of gangliosides was not detected by HPTLC in any of the two samples.

One fucosylated disialoganglioside, Fuc-GD1 (t18:1/24:0), makes the difference between the two samples. Six trisialogangliosides were detected only in the Neo16 ganglioside mixture including 2 fucosylated and 1 *O*-acetylated

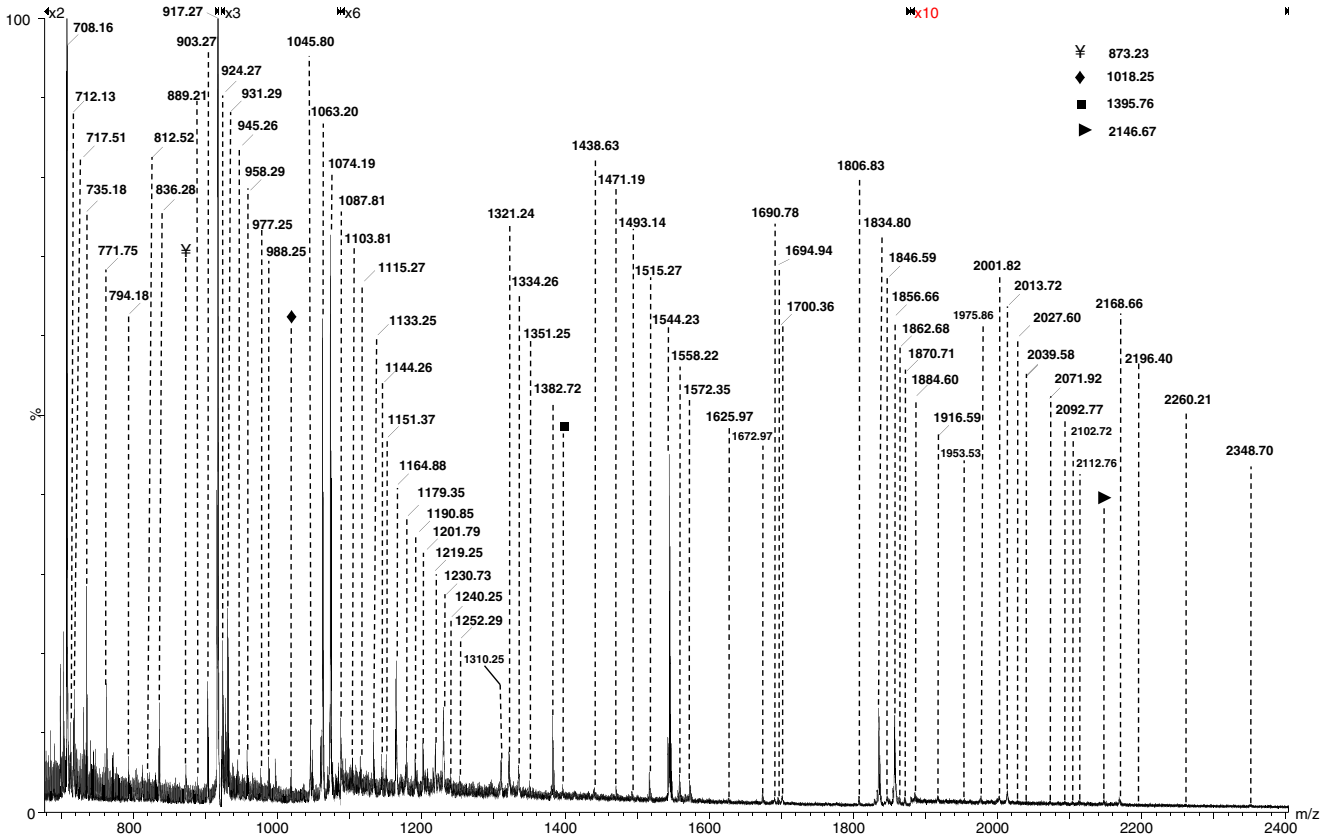

Fig. 2 Negative nanoESI-QTOF MS of Neo14 sample. Cone voltage: 35–50 V. Capillary voltage: 1.8 kV. Acquisition: 300 scans. Argon pressure: 12 p.s.i

species: GT1(t18:0/20:0), Fuc-GT3 (t18:0/18:0), Fuc-GT3 (t18:1/18:0), GT1 (d18:1/16:2), GT1 (t18:0/20:0) and O-Ac-GT1 (t18:1/22:1). Two fucosylated tetrasialo components were also discovered exclusively in the Neo16 sample: Fuc-GQ1 (t18:1/20:1) and Fuc-GQ1 (d18:1/20:2).

Interestingly, altogether three pentasialylated species, of low abundance, were discovered, of which two are common for both samples. A pentasialoganglioside with an uncommon ceramide composition, GP1(t18:1/24:2), detected as $[M+Na^{+}-3H^{+}]^{2-}$ at *m/z* 1,413.23 is apparently associated only to Neo16 since it was not discovered in Neo14 (Table 2). Interestingly, by HPTLC analysis GP species were not detected most probably because of their low expression in the tissue, situated below the detection limit of this method.

It was previously demonstrated that a direct correlation between ganglioside sialylation degree and brain developmental stage exists [11, 17, 18, 22, 34]. Higher sialylation was found specific for incipient developmental stages. Remarkably, in this study, both of the ganglioside mixtures contain structures with a high sialylation degree, up to pentasialo. This feature correlates the clinical developmental stage *i.e.* fetal brains in the beginning of the second trimester of intrauterine life. Nevertheless, obvious differences can be easily noticed, although there is a development difference of only 2 weeks between the two brains. The elevated expression of monosialylated structures in the Neo16 sample versus the Neo14 and the presence of a larger number of polysialylated structures in the Neo14, in agreement with the quantitative analysis, constitues a clear marker of the development-dependant changes in the sialylation profile; the younger brain exhibits a higher number of polysialylated structures. Moreover these results indicate for the first time that the modifications in ganglioside sialylation might begin immediately in the intrauterine life and have a relatively rapid progression. In addition, ganglioside chains modified by labile attachments, such as Fuc and *O*-Ac, were previously reported as being associated with the tissue during its later fetal developmental phase [35]. Thus, while the number of fucosylated species is comparable in both samples, the number of *O*-acetylated differs. In Neo14 sample, 8 % of the total number of gangliosides are *O*-acetylated, but after only two weeks of development, in the Neo16 sample, 10 % of structures are *O*-acetylated. Presumably, the *O*-acetylation process modifies faster than fucosylation, documenting better the brain developmental evolution. Certainly, these findings open a new research direction for the elucidation of the

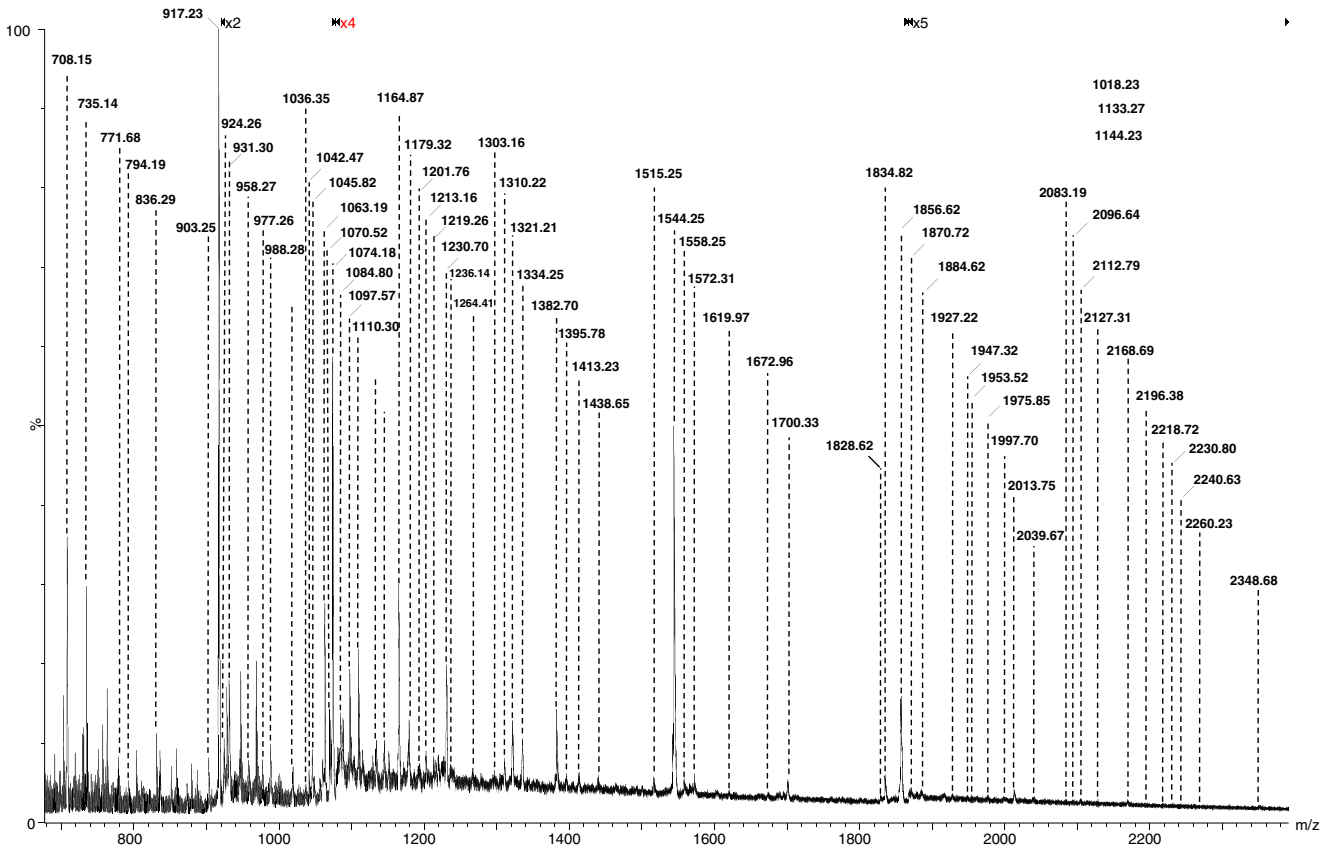

Fig. 3 Negative nanoESI-QTOF MS of Neo16 sample. Cone voltage: 35–50 V. Capillary voltage: 1.8 kV. Acquisition: 300 scans. Argon pressure: 12 p.s.i

precise role of ganglioside fucosylation and acetylation in fetal brain development.

Fragmentation analysis by CID MS/MS

For structural analysis, we selected GM1 (d18:1/18:0), GT1 (d18:1/18:0) and Fuc-GP1 (d18:1/18:0) from Neo14 and Neo16. The option for these three gangliosides exhibiting the same ceramide was guided by their presence in both samples possibly by the action of sialyl- and fucosyltransferases upon GM1 (d18:1/18:0). The experimental conditions were in all cases thoroughly optimized to induce not only the fragmentation of the carbohydrate chain but also of the lipid moiety. Since almost identical results were obtained for the three species from both mixtures, we have chosen to present only one set of data (Neo14).

The singly charged species $[M\text{-}H^+]^-$ at *m/z* 1,544.23, which according to mass calculation corresponds to GM1 (d18:1/18:0) was isolated within an isolation window with LM 10 and HM 10 and was submitted to detailed structural investigation by fragmentation using CID MS/MS. The spectrum generated under variable collision energy within 30–80 eV is depicted in Fig. 4 together with the fragmentation scheme in Fig. 5. The conditions chosen for sequencing enabled the generation of the entire series of B and Z ions together with the counterpart Y and C series identified as signals of fair intensity [35]. The B series encompassing ions from $B_{1\alpha}^-$ at *m/z* 161.01 and its dehydrated from $B_{1\alpha}^-$–H_2O at *m/z* 143.02 to B_4^-–H_2O at *m/z* 983.52 and $B_{1\beta}^-$ at *m/z* 290.05, together with the Z series which includes ions from Z_0^- at *m/z* 546.52 to $Z_{3\alpha}^-$–H_2O at *m/z* 1,346.89 and its sodiated form $[Z_{3\alpha}+Na^+ -2H^+]^-$–$H_2O$ at *m/z* 1,368.32 and $Z_{1\beta}^-$ at *m/z* 1,253.66 confirm the molecular structure proposed. Also, the C series, from $C_{1\alpha}^-$ and its sodiated form $[C_{1\alpha}+Na^+\text{-}2H^+]^-$ at *m/z* 179.02 and *m/z* 201.05 to $[C_4+Na^+\text{-}2H^+]^-$- H_2O at *m/z* 1,023.57 and $C_{1\beta}^-$ with its sodiated form $[C_{1\beta}+Na^+\text{-}2H^+]^-$ at *m/z* 308.23 and *m/z* 331.08 along with the Y series encompassing ions from Y_0^- and *m/z* 564.51 to $Y_{3\alpha}^-$ at *m/z* 1,382.60 also support GM1 structure. Besides the classical glycosidic bond cleavages, some with the preservation of the Neu5Ac, a number of double bond cleavages of high structural relevance were induced under the optimized sequencing conditions. These cleavages generated $[Y_{2\alpha}/Z_1+Na^+\text{-}2H^+]^-$-$H_2O$ at *m/z* 474.27, $[Y_{2\alpha}/B_{1\beta}]^-$ at *m/z* 888.57 and $[Y_{3\alpha}/B_{1\beta}]^-$ together with its dehydrated form $[Y_{3\alpha}/B_{1\beta}]^-$- H_2O at *m/z* 1,091.57 and *m/z* 1,073.78 ions.

The ceramide composition was also documented by the derived fragment ions produced within the same

Table 2 Comparative assignment of the major ions detected in the Neo14 and Neo16 samples. Detection limit 1 μg

m/z	Molecular ion	Proposed structure	Neo 14	TLC visibility	Neo 16	TLC visibility
1036.35	$[M-H^+]^-$	GM4 (t18:0/18:0)	-	↓	+	↓
1042.47	$[M-H^+]^-$	GM4 (d18:1/20:2)	-		+	
1070.52	$[M-H^+]^-$	GM4 (d18:1/22:2)	-		+	
1110.30	$[M-H^+]^-$	*O*Ac-GM4(d18:1/22:03)	-		+	
1179.35	$[M-H^+]^-$	GM3(d18:1/18:0)	+	↑	+	↑
1213.16	$[M+Na^+-2H^+]^-$	GM3 (t18:1/18:2)	-		+	
1236.14	$[M-H^+]^-$	GM3(d18:1/22:0)	-		+	
1252.29	$[M-H^+]^-$	*O*Ac-GM3(d18:0/20:0)	+		-	
1264.41	$[M-H^+]^-$	GM3(d18:1/24:0)	-		+	
1351.25	$[M-H^+]^-$	GM2 (d18:1/16:2)	+	↑	-	↑
1382.72	$[M-H^+]^-$	GM2 (d18:1/18:0)	+		+	
771.75	$[M-2H^+]^{2-}$	GM1(d18:1/18:0)	+	↑	+	↑
794.18	$[M-2H^+]^{2-}$	GM1(t18:1/20:0)	+		+	
1544.23	$[M-H^+]^-$	GM1(d18:1/18:0)	+		+	
1558.22	$[M-H^+]^-$	*O*Ac-GM1(d18:1/16:0)	+		+	
1572.35	$[M-H^+]^-$	GM1(d18:1/20:0)	+		+	
1619.97	$[M-H^+]^-$	GM1(d18:0/24:0)	-		+	
1625.97	$[M-H^+]^-$	GM1(d18:1/24:2)	+		-	
1690.78	$[M-H^+]^-$	Fuc-GM1(d18:1/18:0)	+		-	
1700.36	$[M-H^+]^- - H_2O$	Fuc-GM1(d18:1/20:0)	+		+	
735.18	$[M-2H^+]^{2-}$	GD3 (d18:1/18:0)	+	↑	+	↑
1471.19	$[M-H^+]^-$	GD3(d18:1/18:0)	+		-	
1493.14	$[M+Na^+-2H^+]^-$	GD3 (d18:1/18:0)	+		-	
1515.27	$[M-H^+]^-$	GD3 (t18:1/20:0)	+		+	
836.26	$[M-2H^+]^{2-}$	GD2 (d18:1/18:0)	+	↑	+	↑
889.21	$[M+Na^+-3H^+]^{2-}$	GD2 (d18:1/24:0)	+		-	
1672.97	$[M-H^+]^-$	GD2(d18:1/18:1)	+		+	
1694.94	$[M+Na^+-2H^+]^-$	GD2(d18:1/18:1)	+		+	
903.27	$[M-2H^+]^{2-}$	GD1(d18:1/16:0)	+	↑	+	↑
917.27	$[M-2H^+]^{2-}$	GD1(d18:1/18:0)	+		+	
924.27	$[M-2H^+]^{2-}$	GD1 (t18:1/18:1)	+		+	
928.28	$[M+Na^+-3H^+]^{2-}$	GD1(d18:1/18:0)	+		+	
931.29	$[M-2H^+]^{2-}$	GD1(d18:1/20:0)	+		+	
938.27	$[M-2H^+]^{2-}$	GD1(t18:1/20:1)	+		-	
945.26	$[M-2H^+]^{2-}$	GD1(d18:1/22:0)	+		-	
958.29	$[M-2H^+]^{2-}$	GD1(d18:1/24:1)	+		+	
977.25	$[M-2H^+]^{2-}$	Fuc-GD1(d18:0/16:0)	+		+	
988.25	$[M-2H^+]^{2-}$	Fuc-GD1(d18:1/18:2)	+		+	
1018.25	$[M-2H^+]^{2-}$	Fuc-GD1 (d18:1/22:0)	+		+	
1834.80	$[M-H^+]^-$	GD1 (d18:1/18:0)	+		+	
1856.66	$[M+Na^+-2H^+]^-$	GD1 (d18:1/18:0)	+		+	
1862.68	$[M-H^+]^-$	GD1 (d18:1/20:1)	+		-	
1870.71	$[M+Na^+-2H^+]^-$	GD1 (t18:1/18:2)	+		+	
1884.60	$[M+Na^+-2H^+]^-$	GD1 (d18:1/20:1)	+		+	
2013.72	$[M-H^+]^-$	Fuc-GD1 (d18:0/20:0)	+		+	
2027.60	$[M-H^+]^-$	Fuc-GD1 (t18:1/20:0)	+		-	
2039.58	$[M-H^+]^-$	Fuc-GD1 (d18:1/22:0)	+	↑	+	↑
2071.92	$[M+2Na^+-3H^+]^-$	Fuc-GD1 (t18:1/20:0)	+		-	
2083.19	$[M-H^+]^-$	Fuc-GD1 (t18:1/24:0)	-		+	
1806.83	$[M-H^+]^-$	GT3(t18:1/20:0)	+	↓	-	↓

Table 2 (continued)

m/z	Molecular ion	Proposed structure	Neo 14	TLC visibility	Neo 16	TLC visibility
1828.64	$[M\text{-}H^+]^-$	*O*Ac-GT3 (d18:1/18:0)	+		+	
1846.59	$[M\text{-}H^+]^-$	GT3(d18:1/24:0)	+		-	
1916.59	$[M+Na^+\text{-}2H^+]^-$	Fuc-GT3 (t18:1/16:1)	+		+	
1927.22	$[M\text{-}H^+]^-$	Fuc-GT3 (t18:0/18:0)	-		+	
1947.32	$[M+Na^+\text{-}2H^+]^-$	Fuc-GT3 (t18:1/18:0)	-		+	
1953.53	$[M\text{-}H^+]^-$	Fuc-GT3 (t18:1/20:0)	+		+	
1975.86	$[M+Na^+\text{-}2H^+]^-$	Fuc-GT3 (t18:1/20:0)	+		+	
1997.70	$[M+2Na^+\text{-}3H^+]^-$	Fuc-GT3 (t18:1/20:0)	-		+	
2001.82	$[M\text{-}H^+]^-$	Fuc-GT3 (t18:1/24:4)	+		-	
1059.28	$[M\text{-}2H^+]^{2-}$	Fuc-GT2(t18:1/18:4)	+	↓	+	↓
1069.27	$[M\text{-}2H^+]^{2-}$	Fuc-GT2(d18:1/20:0)	+		-	
2092.77	$[M\text{-}H^+]^-$	Fuc-GT2 (t18:1/16:4)	+		-	
2124.78	$[M\text{-}H^+]^-$	Fuc-GT2 (t18:1/18:2)	+		-	
708.16	$[M\text{-}3H^+]^{3-}$	GT1(d18:1/18:0)	+	↑	+	↑
712.13	$[M\text{-}3H^+]^{3-}$	GT1(t18:1/18:2)	+		-	
717.51	$[M\text{-}3H^+]^{3-}$	GT1(d18:1/20:0)	+		-	
1045.80	$[M+Na^+\text{-}3H^+]^{2-}$	GT1 (d18:0/14:0)	+		+	
1048.76	$[M\text{-}2H^+]^{2-}$	GT1 (d18:1/16:1)	+		-	
1063.20	$[M\text{-}2H^+]^{2-}$	GT1 (d18:1/18:0)	+		+	
1074.19	$[M+Na^+\text{-}3H^+]^{2-}$	GT1 (d18:1/18:0)	+		+	
1076.84	$[M\text{-}2H^+]^{2-}$	GT1 (d18:1/20:0)	+		-	
1080.24	$[M+Na^+\text{-}3H^+]^{2-}$	GT1 (t18:1/18:2)	+		-	
1084.80	$[M\text{-}2H^+]^{2-}$	GT1(t18:1/20:0)	+		+	
1087.81	$[M+Na^+\text{-}3H^+]^{2-}$	GT1(d18:1/20:0)	+		+	
1095.30	$[M+Na^+\text{-}3H^+]^{2-}$	GT1(t18:1/20:0)	+		-	
1097.57	$[M+Na^+\text{-}3H^+]^{2-}$	GT1(t18:0/20:0)	-		+	
1103.81	$[M+Na^+\text{-}3H^+]^{2-}$	GT1 (d18:0/22:0)	+		-	
1115.27	$[M+Na^+\text{-}3H^+]^{2-}$	GT1 (d18:1/24:1)	+		+	
1133.25	$[M\text{-}2H^+]^{2-}$	*O*Ac-GT1(t18:1/24:1)	+		+	
1144.26	$[M+Na^+\text{-}3H^+]^{2-}$	*O*Ac-GT1(t18:1/24:1)	+		+	
1151.37	$[M+Na^+\text{-}3H^+]^{2-}$	Fuc-GT1 (t18:1/18:4)	+		+	
1164.88	$[M\text{-}2H^+]^{2-}$	Fuc-GT1 (d18:1/22:0)	+		+	
1190.85	$[M+Na^+\text{-}3H^+]^{2-}$	Fuc-GT1 (d18:0/24:0)	+		+	
1201.79	$[M+2Na^+\text{-}4H^+]^{2-}$	Fuc-GT1 (d18:0/24:0)	+		+	
1208.26	$[M+2Na^+\text{-}4H^+]^{2-}$	Fuc-GT1 (t18:1/24:0)	+		-	
2096.64	$[M\text{-}H^+]^-$	GT1 (d18:1/16:2)	-		+	
2102.72	$[M\text{-}H^+]^-$	GT1 (d18:0/16:0)	+		+	
2112.76	$[M\text{-}H^+]^- – H_2O$	GT1 (d18:0/18:0)	+		+	
2127.31	$[M\text{-}H^+]^-$	GT1 (d18:1/18:0)	-		+	
2146.67	$[M+2Na^+\text{-}3H^+]^-$	GT1 (d18:0/16:0)	+		-	
2168.66	$[M\text{-}H^+]^-$	*O*Ac-GT1 (d18:1/18:1)	+		+	
2196.40	$[M\text{-}H^+]^-$	*O*Ac-GT1 (d18:1/20:1)	+		+	
2218.72	$[M+2Na^+\text{-}3H^+]^-$	GT1 (t18:0/20:0)	-		+	
2230.80	$[M+2Na^+\text{-}3H^+]^-$	GT1 (d18:0/22:0)	-		+	
2240.63	$[M\text{-}H^+]^-$	*O*Ac-GT1 (t18:1/22:1)	-	↑	+	↑
2260.21	$[M\text{-}H^+]^-$	Fuc-GT1 (t18:1/16:1)	+		+	
2348.70	$[M\text{-}H^+]^-$	Fuc-GT1 (t18:0/22:0)	+		+	
812.52	$[M+Na^+\text{-}4H^+]^{3-}$	GQ1(d18:1/18:0)	+	↑	-	↑
873.23	$[M+Na^+\text{-}4H^+]^{3-}$	Fuc-GQ1(t18:1/20:4)	+		-	

Table 2 (continued)

m/z	Molecular ion	Proposed structure	Neo 14	TLC visibility	Neo 16	TLC visibility
1216.22	$[M\text{-}2H^+]^{2-}$	GQ1 (t18:1/18:0)	+		+	
1219.25	$[M+Na^+\text{-}3H^+]^{2-}$	GQ1 (d18:1/18:0)	+		+	
1230.28	$[M+2Na^+\text{-}4H^+]^{2-}$	GQ1 (d18:1/18:0)	+		+	
1240.25	$[M+2Na^+\text{-}4H^+]^{2-}$	GQ1 (t18:0/18:0)	+		-	
1280.27	$[M+2Na^+\text{-}4H^+]^{2-}$	GQ1 (t18:1/24:1)	+		+	
1296.22	$[M\text{-}2H^+]^{2-}$	Fuc-GQ1 (d18:1/20:0)	+		+	
1303.16	$[M\text{-}2H^+]^{2-}$	Fuc-GQ1 (t18:1/20:1)	-		+	
1305.16	$[M+Na^+\text{-}3H^+]^{2-}$	Fuc-GQ1 (d18:1/20:2)	-		+	
1307.13	$[M+Na^+\text{-}3H^+]^{2-}$	Fuc-GQ1 (d18:1/20:0)	-		+	
1310.25	$[M\text{-}2H^+]^{2-}$	Fuc-GQ1 (d18:1/22:0)	+		+	
1321.24	$[M+Na^+\text{-}3H^+]^{2-}$	Fuc-GQ1 (d18:1/22:0)	+		+	
1334.26	$[M+Na^+\text{-}3H^+]^{2-}$	Fuc-GQ1 (d18:1/24:1)	+		+	
1395.76	$[M\text{-}2H^+]^{2-}$	GP1(d18:1/24:1)	+	↓	+	↓
1413.23	$[M+Na^+\text{-}3H^+]^{2-}$	GP1(t18:1/24:2)	-		+	
1438.63	$[M+Na^+\text{-}3H^+]^{2-}$	Fuc-GP1 (d18:1/18:0)	+		+	

+ the ion was detected; − the ion was not detected; d-dihydroxylated sphingoid base; t-trihydroxylated sphingoid base; ↑ visible in TLC; ↓ not visible in TLC

tandem MS experiment. U^- at *m/z* 283.26 and S^- at *m/z* 326.20 were detected with fair abundance and contributed to the confirmation of the (d18:1/18:0) structure (Figs. 4 and 10).

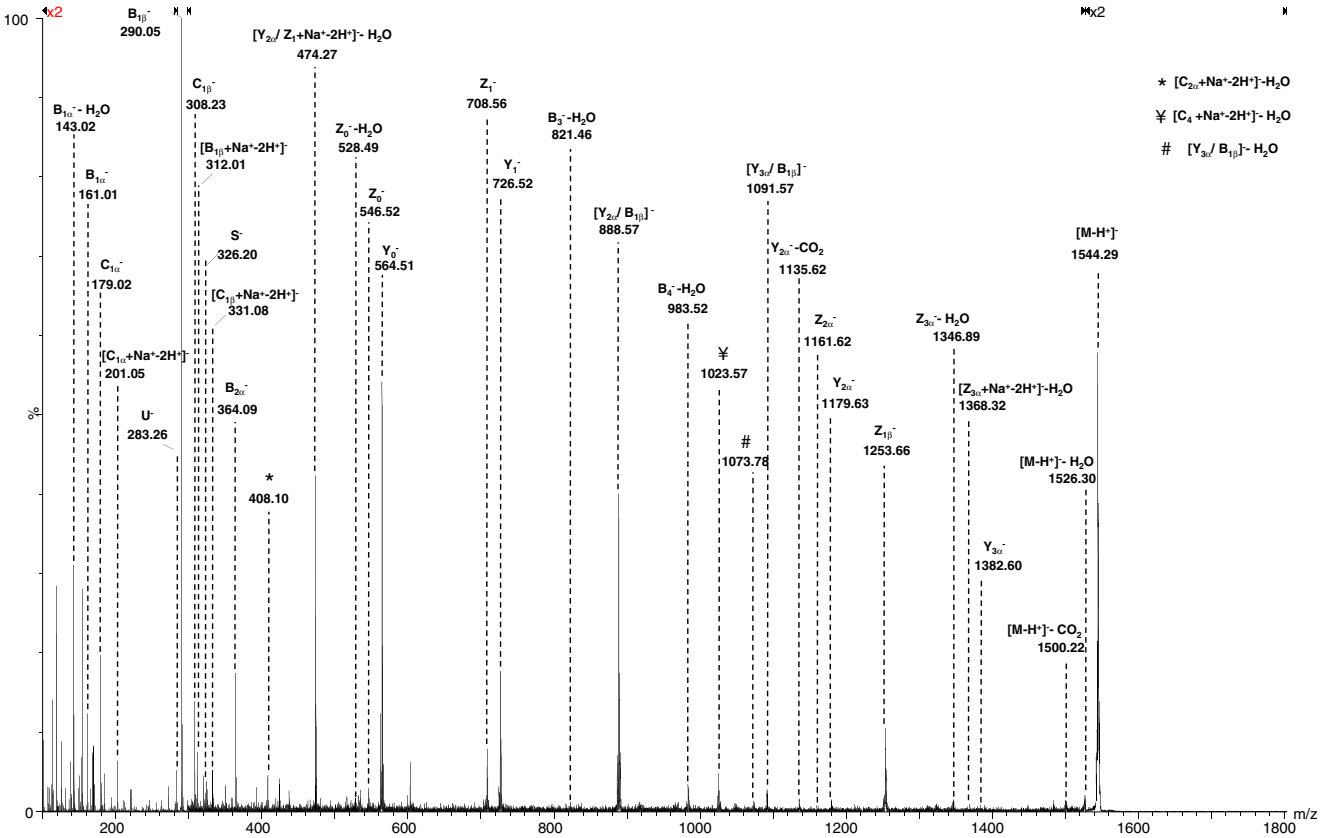

Fig. 4 Negative nanoESI-QTOF CID MS/MS of the singly charged ion $[M\text{-}H^+]^-$ at *m/z* 1,544.29 corresponding to GM1 (d18:1/18:0) fragmented from Neo14 sample. Cone voltage 35 V. Capillary voltage 1.8 kV. Acquisition 300 scans. CID at variable collision energy within 30–60 eV. Argon pressure: 12 p.s.i

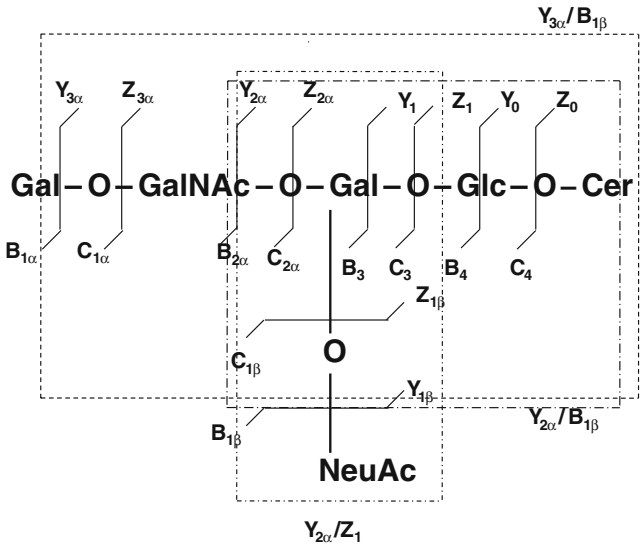

Fig. 5 Fragmentation scheme of GM1 species

GT1 (d18:1/18:0) was identified as the doubly charged species $[M+Na^+-3H^+]^{2-}$ at *m/z* 1,074.11. This ion was also isolated within an isolation window with LM 10 and HM 10 and was submitted to detailed structural investigation by fragmentation using CID MS/MS. The spectrum generated under variable collision energy within 30–80 eV is depicted in Fig. 6 while the fragmentation scheme is presented in Fig. 7. The assessment of the spectrum indicates the formation of almost the whole typical B and Z series of fragment ions together with the counterpart C and Y fragment ions. A number of product ions bring strong evidence with respect to disialo element linkage at the inner Gal which allows to conclude that GT1b (d18:1/18:0) structure is present in Neo14. The most important ions produced by the cleavage of the glycosidic bond that support this concept are $[Y_{4\alpha}$ or $Y_{1\beta}$ $-2H^+]^{2-}$ at *m/z* 917.46 or its sodiated form $[Y_{4\alpha}$ or $Y_{1\beta}+Na^+-2H^+]^-$ at *m/z* 1,857.89, $Z_{4\alpha}^-$ or $Z_{1\beta}^-$ at *m/z* 1,817.61 together with its sodiated form $[Z_{4\alpha}$ or $Z_{1\beta}+Na^+-2H^+]^-$ at *m/z* 1,839.21. Also $[Y_{3\alpha}+Na^+-2H^+]^-$ at *m/z* 1,695.60 and its doubly dehydrated form $[Y_{3\alpha}+Na^+-2H^+]-2H_2O$ at *m/z* 1,659.64, $Z_{3\alpha}^- - H_2O$ at *m/z* 1,637.53 and $[Z_{2\alpha}+Na^+-2H^+]^-$ at *m/z* 1,474.61 or $Z_{2\alpha}^- - H_2O$ at *m/z* 1,434.52 are diagnostic for the proposed structure. Ions also supporting GT1b are $Z_{2\beta}^-$ at *m/z* 1,526.68, $Y_{2\beta}^-$ at *m/z* 1,544.29 or its sodiated form $[Y_{2\beta}+Na^+-2H^+]^-$ at *m/z* 1,566.53 and $B_4^- - 2H_2O$ at *m/z* 1,363.69 together with the sodiated form $[B_4+Na^+-2H^+]^- - H_2O$ at *m/z* 1,403.24. Several double bond cleavage ions such as $[Y_{2\alpha}/B_{2\beta}]^-$ at *m/z* 888.60, $[Y_{3\alpha}/B_{2\beta}]^-$ at *m/z* 1,091.79, $[Y_{4\alpha}/B_{2\beta}]^-$ at *m/z* 1,253.67 and $[Y_{3\alpha}/B_{1\beta}]^-$ at *m/z* 1,382.58, support as well GT1b incidence in Neo14. The ceramide structure is also

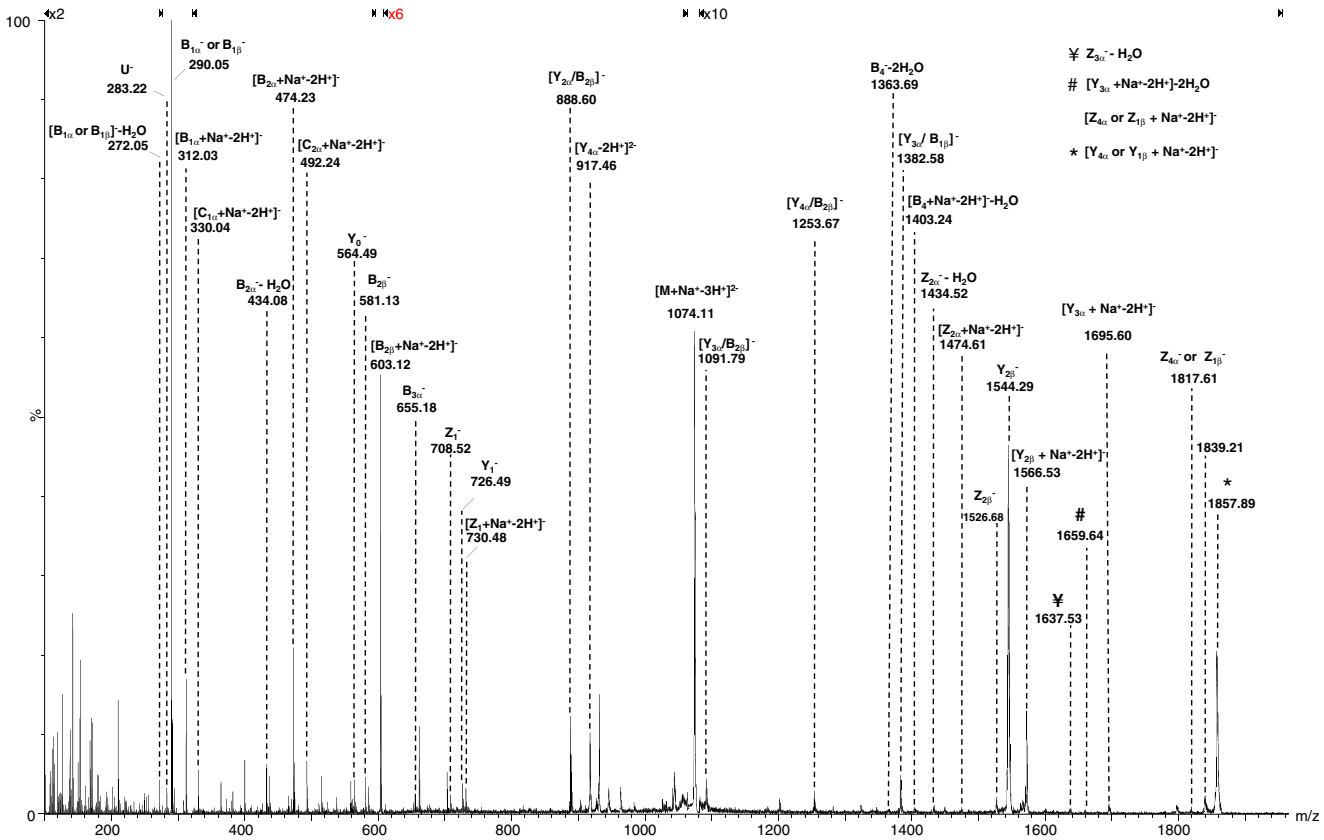

Fig. 6 Negative nanoESI-QTOF CID MS/MS of the doubly charged ion $[M+Na^+-3H^+]^{2-}$ at *m/z* 1,074.11 corresponding to GT1 (d18:1/18:0) fragmented from Neo14 sample. Cone voltage 35 V. Capillary voltage 1.8 kV. Acquisition 300 scans. CID at variable collision energy within 30–60 eV. Argon pressure: 12 p.s.i

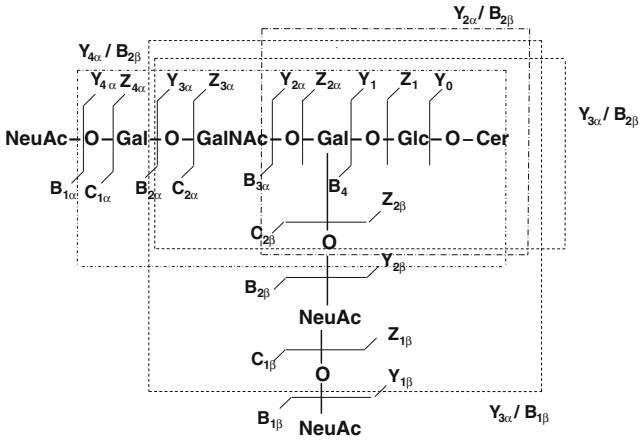

Fig. 7 Fragmentation scheme of GT1b species

confirmed by Y_0^- at *m/z*=564.49 and U^- at *m/z*=283.22 (Figs. 6 and 10).

According to mass calculation the doubly charged species $[M+Na^+-3H^+]^{2-}$ at *m/z* 1,438.63 corresponds to Fuc-GP1 (d18:1/18:0). To analyze in details the structure of this highly unusual ganglioside molecule, the ion was isolated within an isolation window with LM 10 and HM 10 and was submitted to fragmentation using CID MS/MS. The spectrum generated under variable collision energy within 30–80 eV is depicted in Fig. 8 together with the fragmentation scheme in Fig. 9. The high number of sequence ions, diagnostic for the proposed structure, observed in the spectrum in Fig. 8 allows concluding that the conditions for ionization and fragmentation were properly optimized to generate high sequence coverage and complete structural data for this type of substrates. Under these conditions, the assessment of the spectrum indicates the formation of several typical B and Z-type fragment ions together with the counterpart C and Y type. $[B_{4\beta}+2Na^+-3H^+]^-$ at m/z 1,207.29 and its doubly dehydrated form $[B_{4\beta}+Na^+-2H^+]^--2H_2O$ at m/z 1,149.36 is consistent with the tetrasialo element $Neu5Ac_4$ indicating that 4 sialic acid residues are linked together in this ganglioside structure. $Z_{2\alpha}^-$ at *m/z* 2,182.87 together with its doubly dehydrated form at *m/z* 2,147.69 and sodiated doubly dehydrated at *m/z* 2,169.77, $[Z_{3\alpha}+Na^+-2H^+]^--2H_2O$ at *m/z* 2,370.86, $Y_{3\alpha}^-$ *m/z* 2,403.39 and $[Y_{4\alpha}$ or $Y_{1\beta}+Na^+-3H^+]^{2-}$ *m/z* 1,293.01 are all supporting the attachment of the tetrasialo element and Fuc to the inner Gal. $[B_4-2H^+]^{2-}$ at *m/z* 1,062.29 together with its sodiated form $[B_4+Na^+-3H^+]^{2-}$ at *m/z* 1,073.30, $[C_4+2Na^+-3H^+]^-$ at *m/z*=2,189.88, $B_5^--2H_2O$ at *m/z* 2,252.68, $[C_5+Na^+-2H^+]^-$ at *m/z* 2,329.06 also document GP1 structure and support the fucosylation of this species. A number of product ions by double and triple cleavage such as $[Y_{2\alpha}/Z_1/B_{3\beta}+2Na^+$

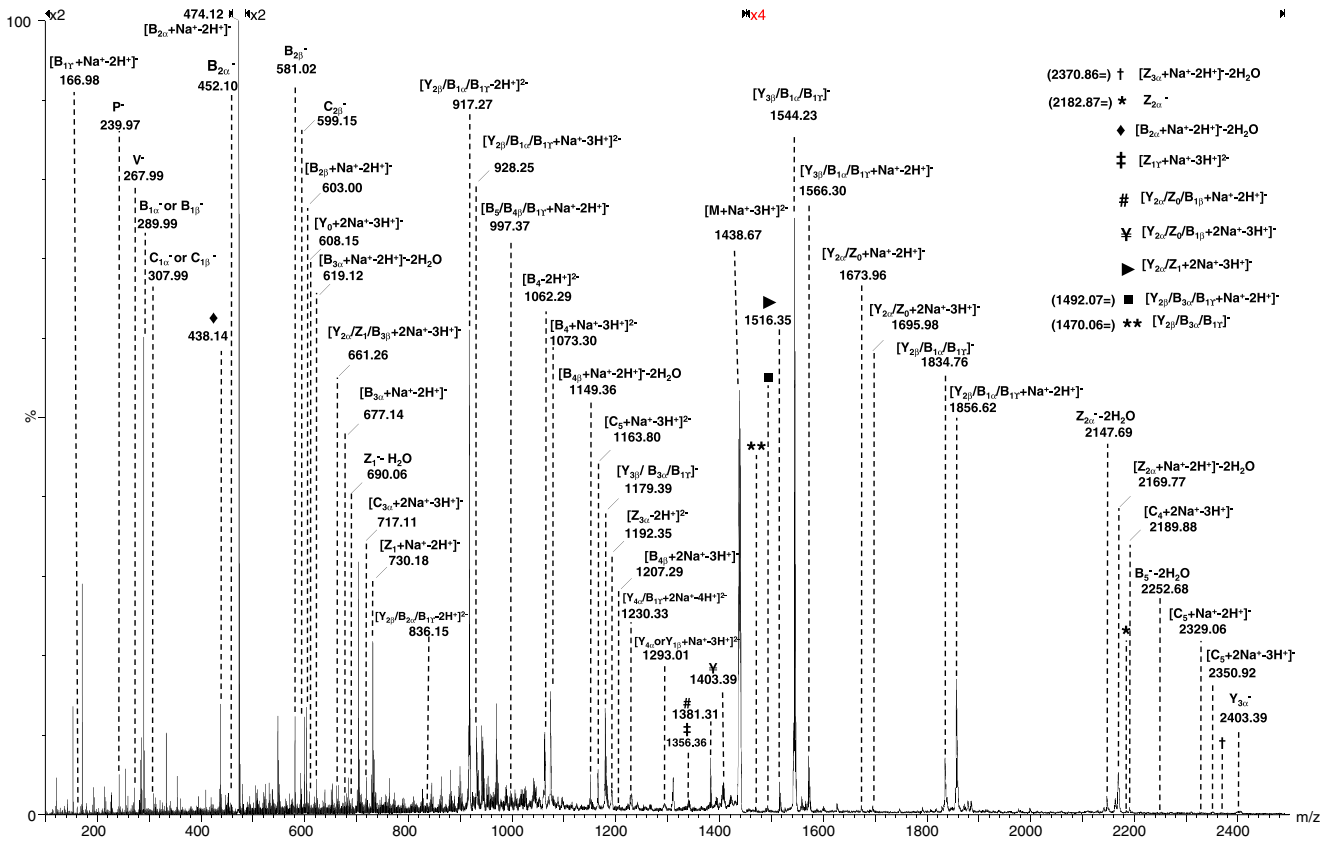

Fig. 8 Negative nanoESI-QTOF CID MS/MS of the doubly charged ion $[M+Na^+-3H^+]^{2-}$ at *m/z* 1,438.63 corresponding to Fuc-GP1 (d18:1/18:0) fragmented from Neo14 sample. Cone voltage 35 V. Capillary voltage 1.8 kV. Acquisition 300 scans. CID at variable collision energy within 30–60 eV. Argon pressure: 12 p.s.i

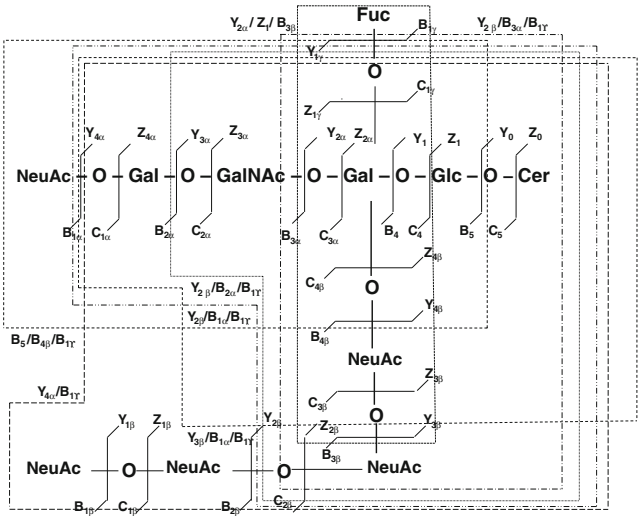

Fig. 9 Fragmentation scheme of Fuc-GP1d species

$-3H^+]^-$ *m/z* 661.26, $[Y_{2\beta}/B_{2\alpha}/B_{1\Upsilon}\text{-}2H^+]^{2-}$ at *m/z* 836.15, $[Y_{2\beta}/B_{1\alpha}/B_{1\Upsilon}\text{-}2H^+]^{2-}$ at *m/z* 917.27, $[Y_{2\beta}/B_{1\alpha}/B_{1\Upsilon}+Na^+\text{-}3H^+]^{2-}$ at *m/z* 928.25, $[B_5/B_{4\beta}/B_{1\Upsilon}+Na^+\text{-}2H^+]^-$ at *m/z* 997.37, $[Y_{3\beta}/B_{3\alpha}/B_{1\Upsilon}\text{-}H^+]^-$ at *m/z* 1,179.39, $[Y_{4\alpha}/B_{1\Upsilon}+2Na^+\text{-}4H^+]^{2-}$ at *m/z* 1,230.33, $[Y_{2\alpha}/Z_0/B_{1\beta}+Na^+\text{-}2H^+]^-$ at *m/z* 1,381.31 and $[Y_{2\alpha}/Z_0/B_{1\beta}+2Na^+\text{-}3H^+]^-$ at *m/z* 1,403.39, $[Y_{2\beta}/B_{3\alpha}/B_{1\Upsilon}]^-$ and $[Y_{2\beta}/B_{3\alpha}/B_{1\Upsilon}+Na^+\text{-}2H^+]^-$ at *m/z* 1,470.06 and 1,492.07 together with $[Y_{2\alpha}/Z_1+2Na^+\text{-}3H^+]^-$ at *m/z* 1,516.35, $[Y_{3\beta}/B_{1\alpha}/B_{1\Upsilon}]^-$ at *m/z* 1,544.23, $[Y_{3\beta}/B_{1\alpha}/B_{1\Upsilon}+Na^+\text{-}2H^+]^-$ at *m/z* 1,566.30, $[Y_{2\alpha}/Z_0+Na^+\text{-}2H^+]^-$ at *m/z* 1,673.96, $[Y_{2\alpha}/Z_0+2Na^+\text{-}3H^+]^-$ at *m/z* 1,695.98 and with $[Y_{2\beta}/B_{1\alpha}/B_{1\Upsilon}]^-$ and $[Y_{2\beta}/B_{1\alpha}/B_{1\Upsilon}+Na^+\text{-}2H^+]^-$ at *m/z* 1,834.76 and 1,856.62 respectively are of highly relevance for the proposed ganglioside structure.

However, due to the symmetry of Gal-GalNAc-Gal chain and the labile attachment of Neu5Ac there are no possible diagnostic ions, even theoretical, able to exclude de occurrence of other isomers. Therefore, although we have demonstrated here for the first time the Fuc-GP1d structure, we cannot eliminate the possible presence in Neo14 or Neo16 of the other GP1 isomers. Interestingly, since in adult human brain the d series was not detected, we assume that the specific sialyltransferase capable to promote this pathway modifies its activity in adulthood. Since a higher sialylation degree is specific for early developmental stages [11, 17, 18, 22, 34] and decreases in time, presumably all sialyltransferases change and/or reduce their activity with brain maturation. However this concept seems not to be valid for fucosyltransferases; we have previously shown that fetal brain in an advanced developmental stages [16], as well as adult human brain [36] exhibit fucosylated species. Apparently, fucosyltransferases continue their activity after birth.

Interestingly, though the carbohydrate chain of GP1 species is particularly long and requires special conditions for sequencing, some ions diagnostic for the ceramide such as P^- at *m/z* 239.97, V^- at *m/z* 267.99, and $[Y_0+2Na^+\text{-}3H^+]^-$ at *m/z* 608.15 could also be detected in the CID experiment in Figs. 8 and 10.

From the methodological point of view for an identical instrumental setup in terms of ionization mode, applied voltages, desolvation temperature, collision energy, gas pressure, acquisition time and the preset resolution, the method provided an excellent reproducibility: 100 % in-run, around 98 % run-to-run and 95 % day-to-day reproducibility of the data, for a number of replicates of at least 3. As under the employed conditions, the measured nanoESI flow rate was about 200 nL/min, considering an approximate sample concentration of 2 pmol/μL, 300 scans which corresponds to 5.0 min signal acquisition is equivalent with a consumption around 2 pmols for a full scan mass spectrum and 2 pmols for a CID MS/MS.

Conclusions

High resolution mass spectrometry was applied for the investigation of two native ganglioside mixtures, extracted from normal human fetal neocortex in the 14th and 16th gestational weeks. MS screening enabled the identification in Neo14 and Neo16 mixtures of 75 and respectively 71 glycoforms with a high degree of heterogeneity in their oligosaccharide sequences and ceramide motifs. Obtained results indicated differences in the expression of mono/polysialylated as well as of *O*-acetylated species in the two ganglioside mixtures which support earlier hypothesis regarding the direct correlation between the sialylation and acetylation degree and brain developmental stage: a higher sialylation degree being specific for incipient developmental stages while a higher acetylation for more developed brains. Our findings are in agreement with the results of Orczyk-Pawiłowicz *et al*. [37] who have studied the amniotic IgA structure during the same gestational stage *i.e*. the second trimester. According to these previous results, high degrees of sialylation and fucosylation are characteristic for early intrauterine development.

The structural confirmation of three gangliosides having the same ceramide composition but differing by their oligosaccharide sequences was achieved by CID MS/MS under variable collision energy. The optimized fragmentation conditions induced efficient ion dissociation with high sequence

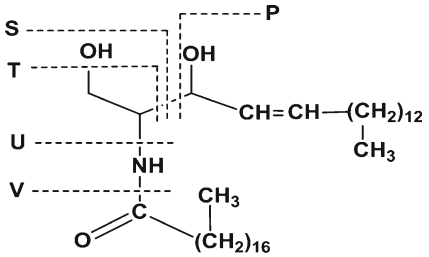

Fig. 10 Fragmentation scheme of the ceramide moiety

coverage and ions diagnostic for the proposed structures of the sugar core and ceramide moiety. Hence, CID MS/MS was successfully applied for the first time to fragmentation analysis of a pentasiaylated ganglioside, Fuc-GP1 (d18:1/18:0), with the first identification in human brain of a GP1d isomer.

We consider that these preliminary findings may provide a solid platform for further development of MS-based methodologies focused on the determination of ganglioside expression and role in fetal brain development and maturation.

Acknowledgements This work was supported by the European Social Fund, through the project POSDRU 107/1.5/S/78702, EU FP7 MARIE CURIE-PIRSES-GA-2010-269256 and by the Romanian National Authority for Scientific Research through the projects PN-II-ID-PCE-2011-3-0047 and PN-II-PCCA-2011-142.

References

1. Lui, J.H., Hansen, D.V., Kriegstein, A.R.: Development and evolution of the human neocortex. Cell **146**(1), 18–36 (2011)
2. Zeng, H., Shen, E.H., Hohmann, J.G., Oh, S.W., Bernard, A., Royall, J.J., Glattfelder, K.J., Sunkin, S.M., Morris, J.A., Guillozet-Bongaarts, A.L., Smith, K.A., Ebbert, A.J., Swanson, B., Kuan, L., Page, D.T., Overly, C.C., Lein, E.S., Hawrylycz, M.J., Hof, P.R., Hyde, T.M., Kleinman, J.E., Jones, A.R.: Large-scale cellular-resolution gene profiling in human neocortex reveals species-specific molecular signatures. Cell **149**, 483–496 (2012)
3. Ronan, L., Voets, N., Rua, C., Alexander-Bloch, A., Hough, M., Mackay, C., Crow, T.J., James, A., Giedd, J.N., Fletcher, P.C.: Differential tangential expansion as a mechanism for cortical gyrification. Cereb. Cortex (2013). doi:10.1093/cercor/bht082
4. Van Essen, D.C., Drury, H.A., Joshi, S., Miller, M.I.: Functional and structural mapping of human cerebral cortex: solutions are in the surfaces. Proc. Natl. Acad. Sci. U. S. A. **95**, 788–795 (1998)
5. Svennerholm, L.: Ganglioside designation. Adv. Exp. Med. Biol. **125**, 125–211 (1980)
6. Tettamanti, G.: Ganglioside/glycosphingolipid turnover: new concepts. Glycoconj. J. **20**, 301–317 (2004)
7. Sonnino, S., Mauri, L., Chigorno, V., Prinetti, A.: Gangliosides ascomponents of lipid membrane domains. Glycobiology **17**(1), 1R–13R (2006). doi:10.1093/glycob/cwl052
8. Yu, R.K., Nakatani, Y., Yanagisawa, M.: The role of glycosphingolipid metabolism in the developing brain. J. Lipid Res. **50**, 440–445 (2009)
9. McJarrow, P., Schnell, N., Jumpsen, J., Clandinin, T.: Influence of dietary gangliosides on neonatal brain development. Nutr. Rev. **67**, 451–463 (2009)
10. Ledeen, R.W.: Gangliosides of the neuron. Trends Neurosci. **8**, 169–174 (1985)
11. Svennerholm, L.: Identification of the accumulated ganglioside. Adv. Genet. **44**, 33–41 (2001)
12. Ngamukote, S., Yanagisawa, M., Ariga, T., Ando, S., Yu, R.K.: Developmental changes of glycosphingolipids and expression of glycogenes in mouse brains. J. Neurochem. **103**, 327–341 (2007)
13. Saito, M., Mao, R.F., Wang, R., Vadasz, C.: Effects of gangliosides on ethanol-induced neurodegeneration in the developing mouse brain. Alcohol. Clin. Exp. Res. **31**, 665–674 (2007)
14. Okada, T., Wakabayashi, M., Ikeda, K., Matsuzaki, K.: Formation of toxic fibrils of Alzheimer's amyloid beta-protein-(1–40) by monosialoganglioside GM1, a neuronal membrane component. J. Mol. Biol. **371**, 481–489 (2007)
15. Mosoarca, C., Ghiulai, R.M., Novaconi, C.R., Vukelić, Z., Chiriac, A., Zamfir, A.D.: Application of chip-based nanoelectrospray ion trap mass spectrometry to compositional and structural analysis of gangliosides in human fetal cerebellum. Anal. Lett. **44**, 1036–1049 (2011)
16. Serb, A., Schiopu, C., Flangea, C., Vukelić, Ž., Sisu, E., Zagrean, L., Zamfir, A.D.: High-throughput analysis of gangliosides in defined regions of fetal brain by fully automated chip-based nanoelectrospray ionization multi-stage mass spectrometry. Eur. J. Mass Spectrom. **15**, 541–553 (2009)
17. Vukelic, Z., Zarei, M., Peter-Katalinic, J., Zamfir, A.D.: Analysis of human hippocampus gangliosides by fully-automated chip-based nanoelectrospray tandem mass spectrometry. J. Chromatogr. A **1130**, 238–245 (2006)
18. Almeida, R., Mosoarca, C., Chirita, M., Udrescu, V., Dinca, N., Vukelic, Z., Allen, M., Zamfir, A.D.: Coupling of fully automated chip-based electrospray ionization to high-capacity ion trap mass spectrometer for ganglioside analysis. Anal. Biochem. **378**, 43–52 (2008)
19. Zamfir, A., Vukelić, Z., Bindila, L., Peter-Katalinić, J., Almeida, R., Sterling, A., Allen, M.: Fully-automated chip-based nanoelectrospray tandem mass spectrometry of gangliosides from human cerebellum. J. Am. Soc. Mass Spectrom. **15**(11), 1649–1657 (2004)
20. Serb, A.F., Sisu, E., Vukelić, Z., Zamfir, A.D.: Profiling and sequencing of gangliosides from human caudate nucleus by chip-nanoelectrospray mass spectrometry. J. Mass Spectrom. **47**(12), 1561–1570 (2012)
21. Svennerholm, L., Fredman, P.: A procedure for the quantitative isolation of brain gangliosides. Biochim. Biophys. Acta **617**, 97–109 (1980)
22. Vukelić, Ž., Metelmann, W., Müthing, J., Kos, M., Peter-Katalinić, J.: Anencephaly: structural characterization of gangliosides in defined brain regions. J. Biol. Chem. **382**, 259–274 (2001)
23. Svennerholm, L.: Quantitative estimation of sialic acids II. A colorimetric resorcinol-hydrochloric acid method. Biochim. Biophys. Acta **24**, 104–111 (1957)
24. Miettinen, T., Takki-Luukkainen, I.T.: Use of buthylacetate in determination of sialic acid. Acta Chem. Scand. **13**, 656–658 (1959)
25. Flangea, C., Serb, A., Sisu, E., Zamfir, A.D.: Chip-based nanoelectrospray mass spectrometry of brain gangliosides. Biochim. Biophys. Acta **1811**(9), 513–535 (2011)
26. Sisu, E., Flangea, C., Serb, A., Zamfir, A.D.: High-performance separation techniques hyphenated to mass spectrometry for ganglioside analysis. Electrophoresis **32**, 1591–1609 (2011)
27. Svennerholm, L.: Ganglioside designation. Adv. Exp. Med. Biol. **125**, 11 (1980)
28. IUPAC-IUB Joint Commission on Biochemical Nomenclature: Eur. J. Biochem. **257**, 293–298 (1998)
29. Domon, B., Costello, C.E.: A systematic nomenclature for carbohydrate fragmentations in FAB MS/MS of glycoconjugates. Glycoconj. J. **5**, 397–409 (1988)
30. Ann, Q., Adams, J.: Structure determination of ceramides and neutral glycosphingolipids by collisional activation of $[M+Li]^+$ ions. J. Am. Soc. Mass Spectrom. **3**, 260–263 (1992)
31. Flangea, C., Sisu, E., Seidler, D.G., Zamfir, A.D.: Analysis of oversulfation in biglycan chondroitin/dermatan sulfate oligosaccharides by chip-based nanoelectrospray ionization multistage mass spectrometry. Anal. Biochem. **420**, 155–162 (2012)
32. Breimer, M.E., Hansson, G.C., Karlsson, K.A., Larson, G., Leffler, H.: Glycosphingolipid composition of epithelial cells isolated along the villus axis of small intestine of a single human individual. Glycobiology **22**, 1721–1730 (2012)
33. Flangea, C., Fabris, C., Vukelic, Z., Zamfir, A.D.: Mass spectrometry of gangliosides from human sensory and motor cortex. Aus. J. Chem. **66**(7), 781–790 (2013)

34. Saito, M., Sugiyama, K.: Tissue-specific expression of c-series gangliosides in the extraneural system. Biochim. Biophys. Acta **1474**, 88–92 (2000)
35. Kracun, I., Rosner, H., Drnovsek, V., Vukelic, Z., Cosovic, C., Trbojevic-Cepe, M., Kubat, M.: Gangliosides in the human brain development and aging. Neurochem. Int. **20**, 421–431 (1992)
36. Zamfir, A.D., Serb, A., Vukelić, Ž., Flangea, C., Schiopu, C., Fabris, D., Kalanj-Bognar, S., Capitan, F., Sisu, E.: Assessment of the Molecular Expression and Structure of Gangliosides in Brain Metastasis of Lung Adenocarcinoma by an Advanced Approach Based on Fully Automated Chip-Nanoelectrospray Mass Spectrometry. J. Am. Soc. Mass Spectrom. **22**, 2145–2159 (2011)
37. Orczyk-Pawiłowicz, M., Augustyniak, D., Hirnle, L., Kątnik-Prastowska, I.: Lectin-based analysis of fucose and sialic acid expressions on human amniotic IgA during normal pregnancy. Glycoconj. J. **30**(6), 599–608 (2013)